Development of a Droplet Entrainment Model for Vertical Annular-Mist Flows

Kum Ho Han, Jee Min Yoo, Jae Jun Jeong
School of Mechanical Engineering, Pusan National University (PNU)

1. Introduction

Droplets play an important role during the reflood phase of a large-break loss of coolant accident (LBLOCA). When a LBLOCA occurs, primary pressure and coolant inventory reduce very quickly. If the primary pressure falls below a certain level, coolant is injected to the lower plenum by the emergency core cooling system (ECCS). Then the coolant enters the reactor core, which is filled with superheated steam, and the reflood phase begins. In the reflood phase, inverted annular-mist or annular-mist flow is often formed in the fuel rod assembly. In the annular-mist flow, the liquid phase consists of liquid films and droplets. The droplets have excellent heat transfer characteristics since these have a wide surface area per unit volume compared to continuous liquid. For this reason, the droplets has a dramatic effect on the cooling of the fuel rods.

Droplet behaviors are divided into two mechanisms : entrainment and deposition. The droplet entrainment is a phenomenon in which a part of a liquid film is separated by the turbulent gas flow. The detached liquid is entrained into the turbulent gas flow and becomes the droplet. The droplet deposition is a phenomenon where droplets flowing along with the gas deposited into liquid films by turbulence in the gas flow or diffusion.

In this paper, an entrainment rate model for vertical annular-mist flow under low-pressure conditions was developed. Then, the entrained fraction calculated from the new model are compared with that of the existing models, using the component-scale thermal-hydraulic analysis code, CUPID [1].

2. Droplet entrainment rate correlation

2.1 Model set-up

Ishii and Grolmes [2] proposed several possible mechanisms of droplet entrainment by high-velocity gas flow and offered the shearing-off of roll wave is the significant entrainment mechanism when the liquid film Reynolds number is higher than a specified value ($Re_{lf} \geq 160$) [2]. Shearing-off of roll wave is a mechanism in which part of roll wave crests is broken up into the droplets by interfacial friction. Therefore, shearing-off of roll wave is heavily influenced by drag force and surface tension [2].

Hewitt and Govan [3] and Dallman [4] developed an entrainment correlation based on shearing-off of roll wave and the onset of entrainment. They used $(G_{lf} - G_{lfc})$ as their main parameter for the entrainment correlation, where G_{lfc} is critical film mass flux for the onset of entrainment. Therefore $(G_{lf} - G_{lfc})$ is the maximum droplet mass flux that can be generated, and the entrainment has a relationship proportional to $(G_{lf} - G_{lfc})$ [4]. Also, Hewitt and Govan [3] used gas mass flux (G_g) as the major parameter. The effect of gas mass flux on the droplet entrainment can be seen through several experiments. Based on these results, we would like to express the entrainment rate in the form of the following correlations.

$$\dot{m}_E = a\sqrt{(G_{lf} - G_{lfc})G_g}\,We_{lf}^{b}Re_g^{c}\left(\frac{\rho_l}{\rho_g}\right)^{0.5}, \quad (1)$$

where Re_g considers the turbulent gas flow, and We_{lf} is used to consider the surface tension. They are defined as follows:

$$Re_g = \frac{\rho_g j_g D}{\mu_g}, \quad (2)$$

$$We_{lf} = \frac{\rho_l j_{lf}^2 D}{\sigma}, \quad (3)$$

and G_{lfc} is given by the following relationship [5]:

$$G_{lfc} = \frac{\mu_l}{D}[7.3\omega^3 + 44.2\omega^2 - 263\omega + 439], \quad (4)$$

$$\omega = \log_{10}\left(\frac{\mu_l}{\mu_g}\sqrt{\frac{\rho_g}{\rho_l}}\right). \quad (5)$$

2.2 New entrainment rate correlation

The deposition rate is relatively easy to measure, but the entrainment rate is difficult to measure. For this reason, Hewitt and Govan [3] and Okawa [6] developed the entrainment rate model by obtaining the entrainment rate data using the assumption that the entrainment rate same as the deposition rate in an equilibrium state. In contrast, Ueda [7] developed a correlation of the entrainment rate, using the mass conservation equation of film that obtains the entrainment rate from the entrained fraction or film mass flux related to droplet mass. The mass conservation equation of film in annular-mist flow is

$$\frac{dG_{lf}}{dz} = G_l\frac{d(1-E)}{dz} = \frac{4}{D}(\dot{m}_D - \dot{m}_E), \quad (6)$$

where $\dot{m}_E$ is the entrainment rate per unit film area, $\dot{m}_D$ is the deposition rate per unit film, area and E is the entrained fraction defined by

$$E = \frac{W_d}{W_{lf}+W_d}. \quad (7)$$

It means the ratio of the droplet mass flow rate to the total liquid mass flow rate. $\dot{m}_D$ and $\frac{dG_d}{dz}$ are required to calculate the droplet entrainment rate from Eq. (6). $\dot{m}_D$ was calculated from Okawa's deposition correlation [6]. Also, $\frac{dG_d}{dz}$ was estimated from the local film mass flux or local entrained fraction. The experimental data used for the new entrainment rate correlation was summarized in Table I. Gill(1963), Hinkle(1967), Ueda(1979), and Wolf(2001) provide local experimental data by measuring the entrained fraction at various heights.

Whalley(1973) and Barbosa(2001) experiments provide the entrained fraction measured at the exit of a very long pipe, so it can be assumed that the entrainment rate is the same as the deposition rate.

Table I: The experimental data used for the new model

Exp.	D [mm]	P [bar]	T [℃]	No. of data
Gill(1963)	31.8	1.5	25	19
Hinkle(1967)	12.6	6.2	21	88
Ueda(1979)	30.0	1.24	25	42
Wolf(2001)	31.8	2.38	25	96
Whalley(1973)	31.8	1.2~3.4	20	43
Barbosa(2001)	31.8	2.0~5.2	25	27

Based on droplet entrainment rate calculated from Eq. (6), the appropriate coefficient and exponents for Eq. (1) were determined. The new correlation is

$$\dot{m}_E = \mathrm{k}_E\sqrt{(G_{lf}-G_{lfc})G_g}We_{lf}^{0.072}Re_g^{0.292}\left(\frac{\rho_l}{\rho_g}\right)^{0.5}, \quad (8)$$

where, Re_g, We_{lf}, G_{lfc} are defined as Eqs. (2) to (5). $\mathrm{k}_E = 3.196\times10^{-6}$ based on the experimental data in Table I.

Fig. 1 show the comparison of the droplet entrainment rate calculated from Eq. (6) and Eq. (8). The measured entrainment rate was estimated from Eq. (6) and calculated entrainment rate was calculated from Eq. (8). A new correlation shows distributed results, but in most cases, it is included within 50% error..

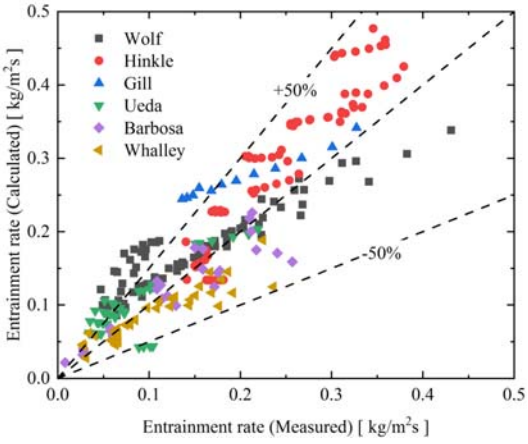

Fig. 1. Comparison of entrainment rate

3. Model assessment

Assessment of new model and existing models was performed with CUPID code using entrained fraction data. The nodalization is done by dividing the test section of each experiment into the same length one-dimensionally. And the inlet mass flow rate and the outlet pressure conditions are applied as boundary conditions.

8 air-water experiments and 2 steam-water experiments performed in the reflood condition were used for the model assessment. The air-water experiments were performed at 1.0~7.6 bar, room temperature, and steam-water experiments were performed at 1.8~3.6 bar, saturated temperature. Selected models and experiments selected are summarized in Tables II and III, respectively.

Table II: The empirical correlations of entrainment rate and deposition rate

Model	Empirical correlations
New Model	$\dot{m}_E = 3.196\times10^{-6}\times\sqrt{(G_{lf}-G_{lfc})G_g}We_{lf}^{0.072}Re_g^{0.292}\left(\frac{\rho_l}{\rho_g}\right)^{0.5}$ $\dot{m}_D = 0.0632\sqrt{\frac{\sigma C}{D}}$ Okawa [1]
Hewitt & Govan [3]	$\dot{m}_E = 5.75\times10^{-5}G_g\left[(G_{lf}-G_{lfc})^2\frac{D\rho_l}{\sigma\rho_g^2}\right]^{0.316}$ $\dot{m}_D = 0.083C\sqrt{\frac{\sigma}{\rho_g D}}max\left(0.3,\frac{C}{\rho_g}\right)^{-0.65}$
Okawa[6]	$\dot{m}_E = 4.79\times10^{-4}\rho_l\frac{f_i\rho_g j_g^2\delta}{\sigma}\left(\frac{\rho_l}{\rho_g}\right)^{0.111}$ $f_i = 0.005\left(1+300\frac{\delta}{D}\right)$ $\dot{m}_D = 0.0632\sqrt{\frac{\sigma C}{D}}$
Kataoka & Ishii [8]	$\dot{m}_E = \left[1200Re_l^{-0.5}Re_{lf\infty}^{-0.25}We^{-1.5}\max(0.0,Re_{lf}-Re_{lf\infty})^2+6.6\times10^{-7}Re_l^{0.74}Re_{lf}^{0.185}We^{0.925}\left(\frac{\mu_g}{\mu_l}\right)^{0.26}\right]\frac{\mu_l}{D}$ $Re_{lf\infty} = Re_l(1-E_\infty)$ $E_\infty = tanh\left(7.25\times10^{-7}We^{1.25}Re_l^{0.25}\right)$ $\mathrm{We} = \frac{\rho_l j_g^2 D}{\sigma}\left(\frac{\Delta\rho}{\rho_g}\right)^{1/3}$ $\dot{m}_D = 0.022G_l Re_l^{-0.25}\left(\frac{\mu_g}{\mu_l}\right)^{0.26}E^{0.74}$

Table III: Sources of entrained fraction data

Exp.	D [mm]	P [bar]	T [℃]	Fluids	No. data
Jagota	25.4	2.8-4.2	21	air-water	27
Whalley	31.8	1.2-3.5	20	air-water	43
Asali	23,42	1.0-2.0	16	air-water	55
Okawa	5.0	1.4-7.6	25	air-water	44
Sawant	9.4	1.2-4.0	25	air-water	30
Barbosa	31.8	2.0-5.2	25	air-water	41
Fore	50.8	1.0	18	air-water	24
Hewitt	9.3	1.8-3.6	Sat	steam-water	71
Yanai	12.0	3.47	Sat	steam-water	21

The entrained fraction calculated from the new correlation and that of the existing correlation were compared with the entrained fraction measured in experiments in Table III to evaluate each correlation. In Fig. 2 ~ 5, the open symbol is the air-water condition and the solid symbol is the steam-water condition. Fig. 2 shows the evaluation results of the new model. The new

model has good predictive performance, with most data included within 30% of deviation. Fig. 3 illustrates that Hewitt-Govan [3] correlation more overpredicts in steam-water data (solid symbol) than air-water data (open symbol). Also, these data are considerable scattering in low entrained fraction region. Fig 4 shows the results calculated from the Okawa [6] correlation is mostly included within 30% compared to air-water data. However, the results underpredict compared to steam-water data. In Fig 5, Kataoka-Ishii correlation clearly shows a considerable under-predict of air-water data and poor prediction of steam-water data.

The root mean square error (RMSE) and the mean absolute percentage error (MAPE) was used to evaluate each droplet model quantitatively, and the assessments are summarized in Table IV. They are defined as follows:

$$\mathrm{RMSE} = \sqrt{\frac{\sum_{i=1}^{N}(\hat{x}_i - x_i)^2}{N}}, \quad (9)$$

$$\mathrm{MAPE}(\%) = \frac{100}{N}\sum_{i=1}^{N}\frac{|x_i - \hat{x}_i|}{|x_i|} \quad (10)$$

where $\hat{x}_i$ is the experimental data and x_i is the predicted value. Table IV shows that the new model has the best results. It also shows that Hewitt and Govan [3] and Okawa [6] model have different results in RMSE and MAPE. This is because the Okawa [6] model predicts well in the low entrained fraction region and not in the high entrained fraction region compared to the Hewitt and Govan [3] model.

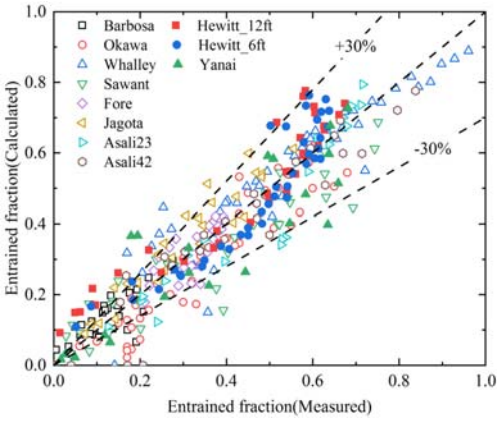

Fig. 2. Comparison of experimental data and new model

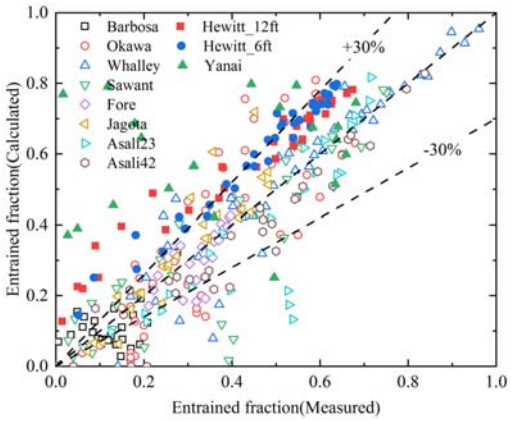

Fig. 3. Comparison of experimental data and Hewitt-Govan model

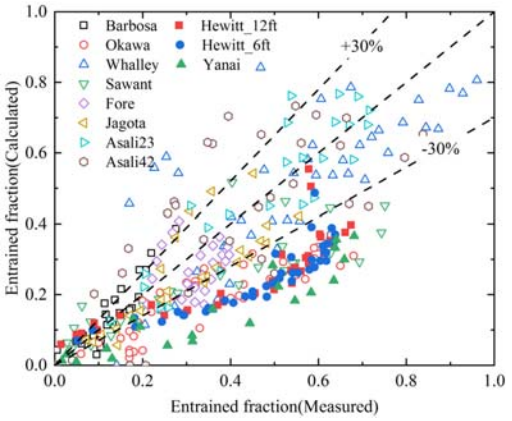

Fig. 4. Comparison of experimental data and Okawa model

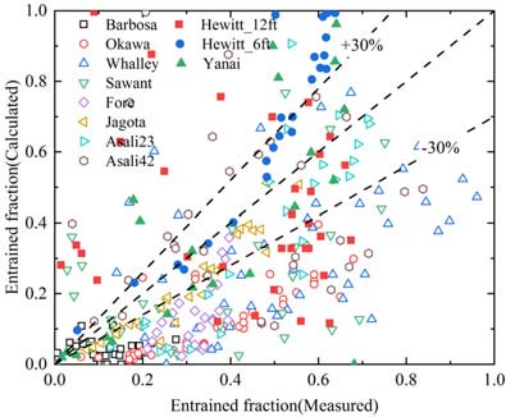

Fig. 5. Comparison of experimental data and Kataoka-Ishii model

Table IV: Quantitatively evaluation of each model

	RMSE	MAPE (%)
New model	0.078	26.12
Hewitt-Govan [3]	0.139	61.35
Okawa [6]	0.172	40.20
Kataoka-Ishii [8]	0.243	75.53

4. Conclusions

A new correlation of the droplet entrainment rate is proposed using the Ueda's assumption [7] and the air-water experimental data in Table I. The new model was compared to the existing model based on the air-water and steam-water experimental data in Table III. The result of the assessment shows that the new model best predicted the experimental data.

Nomenclature

C	droplet concentration (kg/m^3)
D	hydraulic diameter (m)
E	entrained fraction
f_i	interfacial friction factor

G	mass flux (kg/m^2s)
j	superficial velocity (m/s)
m_E	droplet entrainment rate (kg/m^2s)
m_D	droplet deposition rate (kg/m^2s)
Re	Reynolds number
w	mass flow rate (kg/s)
We	Weber number

Greek letters

δ	film thickness (m)
ρ	density (kg/m^3)
σ	surface tension (N/m)
μ	dynamic viscosity ($N\ s/m^2$)

Subscripts

d	droplet
D	deposition
E	entrainment
g	gas
i	interface
l	liquid
lf	liquid film

REFERENCES

[1] J.J. Jeong, H.Y. Yoon, I.K. Park, H.K. Cho, The CUPID Code Development and Assessment Strategy, Nuclear Engineering and Technology, Vol. 40, pp. 636-655, 2010.
[2] M. Ishii., M.A. Grolmes, Inception Criteria for Droplet Entrainment In Two-Phase Concurrent Film Flow, AIChE Journal, Vol 22, pp. 308-318, 1975.
[3] G.F. Hewit, A.H. Govan, Phenomenological Modelling of Non-Equilibrium Flows with Phase Change, International Journal of Heat and Mass Transfer, Vol. 33,pp. 229-242, 1990
[4] J.C. Dallman, Investigation of Separated Flow Model in Annular Gas-Liquid Two-Phase Flows, University of Illinois at Urbana Champaign, PH.D. Thesis, 1978.
[5] C. Berna, A. Escriva, J.L. Munoz-Cobe, L.E. Herranz, Review of Droplet Entrainment in Annular Flow: Interfacial Waves and Onset of Entrainment, Progress in Nuclear Energy, Vol. 74, pp.14-43, 2014.
[6] T. Okawa, A. Kotani, I. Kataoka, M. Naito, Prediction of Critical Heat Flux in Annular Flow Using a Film Flow Model, Journal of Nuclear Science and Technology, Vol. 40, pp.388-396, 2003.
[7] T. Ueda, Entrainment Rate and Size of Entrained Droplets in Annular Two-Phase Flow, Bulletin of JSME, Vol. 22, 1979.
[8] I. Kataoka, M. Ishii, A. Nakayama, Entrainment and Deposition Rates of Droplets in Annular Two-Phase Flow, International Journal of Heat and Mass Transfer, Vol 43, pp.1573-1589, 2000.